SSRG International Journal of Electrical and Electronics Engineering
ISSN: 2348-8379/ https://doi.org/10.14445/23488379/IJEEE-V12I5P106

Volume 12 Issue 5, 58-68, May 2025

Original Article

Optimal Frequency Control of an Autonomous Microgrid Using a Virtual Synchronous Generator Based on the Ant Colony Optimization Algorithm

Hung Nguyen-Van[1*], Hoan Hoang-Van[1], Chuong Trinh-Trong[1]

[1]*Hanoi University of Industry, Hanoi, Vietnam.*

[*]*Corresponding Author : hung_nv@haui.edu.vn*

Received: 01 March 2025 Revised: 06 April 2025 Accepted: 20 April 2025 Published: 31 May 2025

Abstract *- Maintaining frequency stability in isolated microgrids is very challenging due to the unpredictable and fluctuating output of local renewable energy sources, such as wind and solar. Furthermore, given the growing use of distributed generation via power electronics interfaces, the low natural inertia in such systems makes the task more challenging. To solve this issue, the Virtual Synchronous Generator (VSG) is a promising tool for modelling the inertial response of traditional synchronous machines. By adjusting two important parameters, the damping factor D and the virtual moment of inertia J, this paper proposes an optimisation method to enhance the performance of VSG. The Ant Colony Optimisation (ACO) algorithm is used to determine the optimal values for these parameters. Simulation results using MATLAB/Simulink show that the optimised settings significantly improve the microgrid's dynamic frequency behaviour when compared to default control settings, which lowers frequency deviations and speeds up recovery.*

Keywords *- Microgrid, VSG, lack of inertia, ACO, Frequency control.*

1. Introduction

Microgrids are progressively regarded as a viable solution for integrating renewable energy sources into localized power systems. The growing interest is primarily driven by the expanding deployment of Distributed Energy Resources (DERs), particularly solar and wind energy, which are both variable and uncertain in nature [1, 2]. Unlike traditional synchronous generators, these sources are generally linked to the grid through power electronic converters, known as Inverter-Based Resources (IBRs). While IBRs efficiently enable renewable integration, they inherently lack the physical inertia supplied by rotating machines, which is traditionally vital for stabilizing system frequency [3]. The absence of rotational inertia in inverter-based microgrids poses a significant barrier to sustaining frequency stability. In conventional systems, inertial response acts as a natural buffer that limits rapid changes in system frequency during sudden variations in generation or load. IBR-dominated systems have less mechanical inertia, which causes frequency shifts more quickly when the system is perturbed. This can lead to instability, especially during dynamic events. This issue is particularly problematic in isolated or only loosely connected microgrids to the main grid, as even small disturbances can cause large frequency fluctuations. In order to better manage these circumstances, IBRs are typically divided into two categories according to their behavior: Grid-Forming (GFM) and Grid-Following (GFL) inverters. GFM units take the lead, setting both frequency and voltage in a manner similar to that of conventional synchronous machines.GFL inverters, by contrast, follow what's already there, adjusting their current output to match voltage signals from either the main grid or a grid-forming source [4]. These two types rely on quite different control setups. GFM inverters often use two levels of control: one loop on the outside to manage voltage and another inside to regulate current and keep things steady. GFLs, on the other hand, focus on controlling how much power they send, both active and reactive, while also using a current loop for fast responses. Systems with lots of GFLs and no synchronous generators or anything to mimic inertia often have a harder time keeping frequency stable and bouncing back from disturbances [5].

Maintaining consistent frequency, particularly in systems ruled by inverter-based resources, is one of the timeless engineering conundrums in contemporary microgrid design. Unlike conventional grids, which gain from the natural inertia of synchronous generators, these inverter-rich settings lack that stabilizing buffer. The Virtual Synchronous Generator (VSG) idea has gained traction to solve this not only as a workaround but also as a strong tool mimicking the inertial behavior of rotating machines. VSGs support the operational robustness of microgrids more than just maintaining the

frequency steady, thus enabling them to absorb shocks and respond to real-time changes [6]. However, getting the most out of VSGs depends on tuning not only the correct technology but also using the appropriate tools. Every successful VSG's core is a fragile balance of dynamic variables. Chief among them are the damping coefficient (D) and virtual inertia (J).

These aren't just numbers in a control loop; they shape, affecting the system's transient dynamics under disturbances, how quickly it responds, and how gracefully it recovers. Misjudging them could mean sluggish response or, worse, instability when it matters most. Researchers have created simplified models, usually small-signal representations, to assist this design process by facilitating analysis of how such parameters affect system behavior [7]. These models may include representations of a variety of component loads, transmission elements, grid-forming and grid-following inverters, etc., that provide a more comprehensive perspective on system dynamics. However, even with these improvements, obtaining optimal values of VSG parameters is still problematic. The difficulty in the tune equivalent here is due to power systems' nonlinear response and sensitivity to operating point variations [8]. Within these challenges, optimization algorithms have been employed in a number of works to fine-tune VSG control settings. These techniques are proven to be effective in improving the frequency response and helping microgrids maintain stability under various circumstances.

Optimization algorithms have been increasingly used in microgrid systems with VSG technology to improve frequency control performance and the entire system stability. A number of optimization algorithms, including Particle Swarm Optimization (PSO), Genetic Algorithm (GA) and Differential Evolution (DE), have been widely used for optimizing VSG control parameters and have been proven effective. Among them, Ant Colony Optimization (ACO) is one of the promising methods because of its good global search ability. However, the use of ACO for tuning VSG parameters in the context of microgrid frequency control is still in the infancy stage of research, and there is a lack of research that investigates this possibility [9].

In contrast with traditional algorithms (such as PSO, GA and DE), ACO is not commonly used because of its high computational complexity [10]. Although PSO and DE are commonly used due to their high global searching capabilities, ACO has a promising solution of optimizing VSG parameters by adopting virtual inertia and virtual damping coefficients, which affect the frequency stability by adjusting them during the dynamic course [11]. However, ACO has not been able to be widely employed for microgrid applications in real-time due to some issues, including the complex parameters tuning, local optima solution and the high requirement of computation [12, 13]. More investigations are needed for better adaptation and effectiveness of ACO in this area, other than its hybrid variants where ACO is combined with other meta-greedy techniques [14]. The remainder of this paper is structured as follows: section 2 provides the theoretical model for frequency control of microgrids, with special emphasis on the VSG operation principle and the dynamic effect of J and D on system stability. In Section 3, we describe the proposed optimization procedure, which is rooted in the mechanism of the ACO algorithm and provide a mathematical model and search strategy for the determination of control parameters. Section 4 describes a thorough simulation campaign in Matlab/Simulink in order to evaluate the performance of the proposed method compared to fixed parameters configurations under different operating points. Section 5 condenses the main results, critically comments on the limitations via challenges and concludes and provides the possible future research to improve the control performance of VSGs in microgrid scenarios.

2. VSG-Based IBR Model

2.1. Role of Rotational Inertia in Static Stabilization Systems

Rotational inertia is a critical factor closely associated with system stability, particularly frequency stability. The distinction in frequency response between high-inertia and low-inertia power grids is illustrated in Figure 1. Key parameters such as the minimum frequency and the rate of change of frequency (RoCoF) exhibit significant deterioration as system inertia decreases [15].

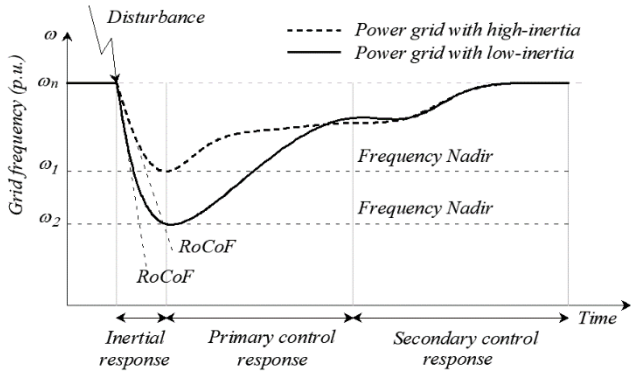

Fig. 1 Comparison of frequency response in low-inertia and high-inertia power grids

The kinetic energy of the rotor in a synchronous generator is determined by:

$$E_r = \frac{1}{2} J \omega_r^2 \quad (1)$$

In which:

J : Rotor inertia moment [$kg.m^2$]

ω_r : Rotor angular velocity [rad/s]

By differentiating Equation (1), the power expression is obtained as:

$$\frac{dE_r}{dt} = J\omega_r \frac{d\omega_r}{dt} \quad (2)$$

Expressing Equation (2) in per-unit form, under the assumption that the rotor angular speed oscillates around the synchronous frequency ω_{ro} *(rad/s)*, a first-order dynamic equation is derived.

$$P_m - P_e = 2H\frac{d\omega_r}{dt} + K_d(\omega_r - \omega_g) \quad (3)$$

$$H = \frac{J\omega_{ro}^2}{2S_{Base}} \quad (4)$$

$$\frac{d\delta}{dt} = \omega_r - \omega_g \quad (5)$$

In which:

P_m : Mechanical power input from the prime mover
P_e : Electrical power output
ω_r : Rotor angular velocity [*rad/s*]
ω_{ro} : Synchronous angular velocity of the rotor [*rad/s*]
ω_g : Reference angular velocity of the grid [*rad/s*]
δ : Rotor angle deviation
S_{Base} : Base apparent power of the generator [*VA*]
H : Inertia constant [*s*]
J : Rotor inertia moment [$kg.m^2$]
D : Damping coefficient
K_d : Synchronizing torque coefficient between the generator and the grid

Equation (3) describes the dynamic relationship between the imbalance of mechanical and electrical power and the resulting variations in rotor speed, which in turn induce frequency oscillations in the power system.

A fundamental parameter governing the stability of these oscillations is the inertial torque, which quantifies the rotational inertia of the generator rotor and serves as a critical determinant of the system's transient and frequency stability.

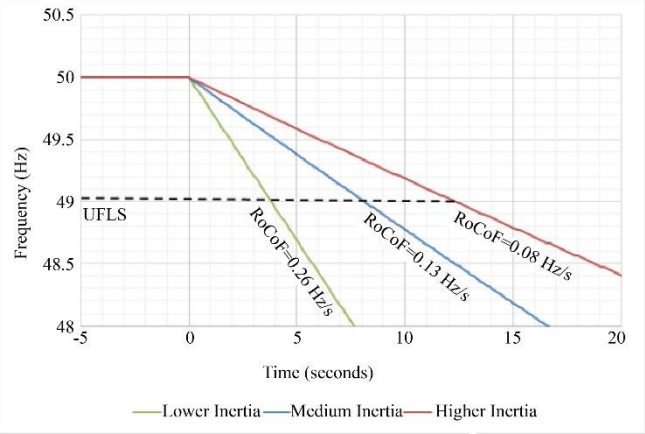

Fig. 1 Impact of inertia reduction

Rotational inertia represents a fundamental component of the power system's stored energy in the form of kinetic energy. This inherent energy storage capability contributes significantly to system stability by mitigating frequency deviations under disturbance conditions. However, with the increasing penetration of IBRs, the aggregate system inertia exhibits a declining trend [16]. A direct consequence of reduced inertia is an increased RoCoF following disturbances, which elevates the risk of maloperation of protective relays and severe frequency excursions, potentially leading to the activation of under-frequency load-shedding schemes [17]. This phenomenon is illustrated in Figure 2.

2.2. IBR Structure Using VSG Controllers

A microgrid with IBRs has a hierarchical structure of processing DERs, including primary and secondary control schemes. The macro control loop contains the VSG, voltage control loop and current control loop. The focus of this paper is frequency regulation and active power sharing. However, the coupling between the voltage control loops and the current control loops yields dynamic couplings, which result in the imbalances of the systems and subsequently influence the stability and performance of the microgrid [4]. Figure 3 depicts the implementation of the VSG control strategy in a voltage-source inverter-based resource.

The Virtual Synchronous Generator (VSG) controller is composed of three main parts: primary control loop, secondary control loop, and virtual inertia loop. The virtual inertia loop is used to mimic the inertia of a typical synchronous generator to support system frequency stability. The first and the second control loops cooperatively regulate the frequency to a target level after an occurrence of active power perturbation, which is manifested as a result of the output power (P_{out}).

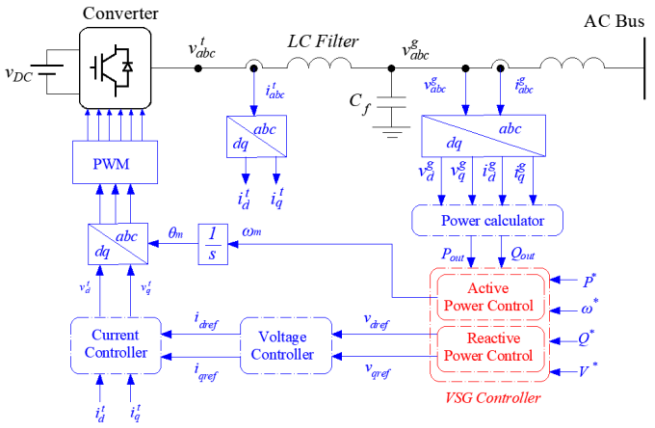

Fig. 2 Structure of IBR utilizing a VSG controller

The virtual inertia controller, which is the virtual inertia system emulating the electromechanical dynamics of a synchronous generator, is incorporated into the control algorithm of the Voltage Source Inverter (VSI) to alleviate the

natural lack of inertia that is typical in the power electronic-based system. This helps IBRs replicate the dynamic characteristics of a conventional synchronous generator and enhances the stability and robustness of the microgrids.

2.2.1. Active Power Control in Synchronous Generators

The *"Active Power Control"* block is structured into two cascaded sub-blocks, representing the *"Governor"* and the *"Swing Equation"* dynamics. The *"Governor"* model, illustrated in Figure 4, is designed based on the droop characteristic, where the proportional gain k_p defines the relationship between *P*-ω.

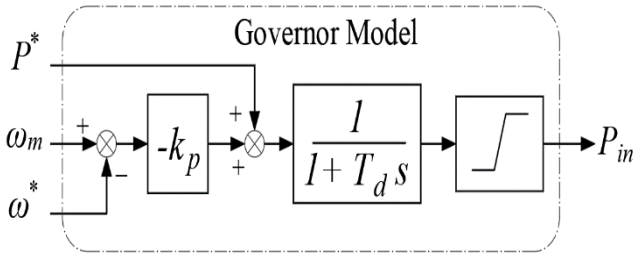

Fig. 4 Governor model

Additionally, a time-delay element with a delay constant T_d is incorporated to emulate the mechanical response delay inherent in the governor system of a conventional synchronous generators.

$$P_{in} = \frac{1}{1+T_D s}\left(P^* - k_p(\omega_m - \omega^*)\right) \quad (6)$$

Following the "Governor" model, the "Swing Equation" model is implemented to represent the electromechanical dynamics of an SG, as depicted in Figure 5. This model characterizes the relationship between mechanical power, electrical power, and rotor dynamics, serving as a fundamental component in emulating the inertial response within the VSG control framework.

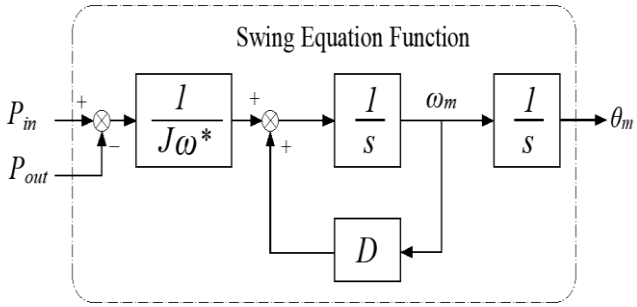

Fig. 5 Model of swing equations

In which:

$$P_{in} - P_{out} = J\omega^* \frac{d\omega_m}{dt} + D(\omega_m - \omega^*) \quad (7)$$

$$\theta_m = \int \omega_m dt \quad (8)$$

2.2.2. Reactive Power Control in Synchronous Generators

In parallel with frequency regulation via active power control, voltage regulation is achieved through reactive power control. The reactive power control mechanism is structured into two sequential stages and is integrated with the inner voltage control loop of the converter controller. The initial stage, implementing Q-V droop control, as illustrated in Figure 6, governs voltage regulation by dynamically adjusting reactive power injection in response to system conditions, thereby enhancing voltage stability and supporting grid operation.

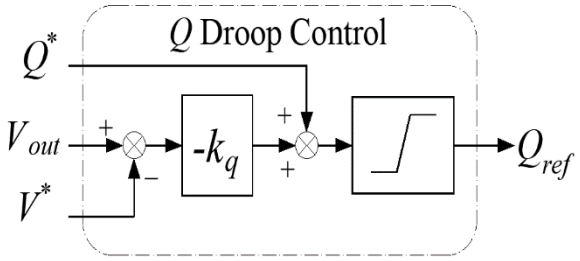

Fig. 6 Reactive power droop control

Following the reactive power droop controller, a Proportional-Integral (PI) reactive power controller is incorporated to emulate the Automatic Reactive Power Regulator in conventional synchronous generators. This PI controller, as depicted in Figure 7, ensures accurate regulation of reactive power, contributing to voltage stability and dynamic support in microgrid operations.

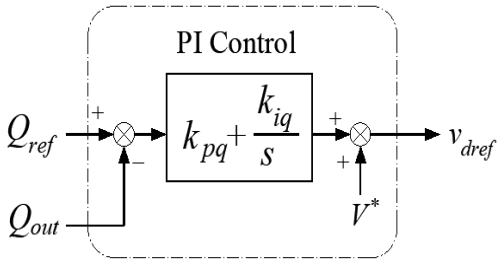

Fig. 7 Reactive power PI controller

In which:

$$Q_{ref} = Q_o - k_q(V_{out} - E^*) \quad (9)$$

$$E_{dref} = E^* + (Q_{ref} - Q_{out}).\left(k_{pq} + \frac{k_{iq}}{s}\right) \quad (10)$$

2.2.3. The Loop Controls Voltage and Current

In grid-connected mode, large-capacity SGs play a crucial role in maintaining microgrid frequency and voltage stability. However, in islanded operations, this responsibility is transferred to internally Distributed Generators (DGs). The control architecture of grid-forming DGs is designed to ensure frequency and voltage regulation, as illustrated in Figure 8. The inner current control loop receives input signals generated

by the outer voltage controller [18]. The outer droop control loop is implemented based on predefined power-sharing coefficients among DGs, yet the control process operates independently within each DG, adhering to grid frequency constraints.

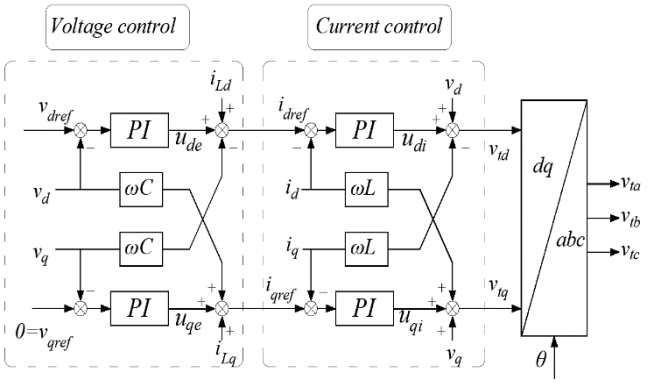

Fig. 8 Voltage and current control loop

The current controller, with state variables representing the output inductance current of the converter, is designed in the rotating *dq-axis* reference frame. The output vector signal of the controller is given by [u_{di}, u_{qi}]:

$$u_{di} = v_{td} + \omega L i_q - V_d \quad (11)$$

$$u_{qi} = v_{tq} - \omega L i_d - V_q \quad (12)$$

The voltage controller, with state variables representing the output capacitor voltage of the converter, is designed in the rotating *dq-axis* reference frame. It is assumed that the dynamic response of the inner current control loop is significantly faster than that of the outer voltage control loop. Therefore, for the voltage control loop, it can be approximated that $i_d \approx i_{dref}$ and $i_q \approx i_{qref}$.

The output vector signal of the controller is given by [u_{di}, u_{qi}]:

$$u_{de} = i_d - i_{Ld} + \omega C V_q \quad (13)$$

$$u_{qe} = i_q - i_{Lq} - \omega C V_d \quad (14)$$

3. Ant Colony Optimization for VSG Parameter Tuning

3.1. Introduce Ant Colony Optimization

Ant Colony Optimization (ACO) was initially proposed by Marco Dorigo himself in his doctoral thesis as a metaheuristic optimization technique that is based on the foraging behavior of ants in the wild [19]. The ability of ants to work together is based on stigmergy, an indirect form of communication in which an individual changes the environment to affect the behavior of another individual. During the search, ants leave behind a chemical, pheromone, through which other ants modify their subsequent paths. In other words, when an ant finds a chemical (pheromone) trail left by a previous ant, it can, with a certain probability, follow the trail, and the more it follows the trail, the more frequently it tends to follow it in the future. It follows that if a path has more pheromones on it, then it is more likely that it is the shortest path, which leads to a self-organizing global behavior that leads to the discovery of the shortest path. However, when a pheromone trail that is part of a suitable solution is not consistently reinforced, it undergoes degradation and direction, and therefore, reduction in influence and 8 exploration of the search space, and this reduces the likelihood of premature convergence on suboptimal solutions [20, 21].

Pheromone updates used to guide ants probabilistically through the search space are employed by the ACO algorithm to polish optimization solutions. The procedure uses a probabilistic state transition rule based on both the intensity of the pheromone and the heuristic desirability. In every cycle, ACO generates a collection of potential solutions and calculates the potential for the subset of the sites in order to estimate the global minimum. Ants specifying more rewarding solutions strengthen their paths with more pheromones, while others are (gradually) abandoned owing to pheromone evaporation. It is through this repetitive process that an appropriate balance between exploration and exploitation is achieved, which allows ACO to be efficient when traversing intricate, multimodal search landscapes.

Algorithm ACO

```
Initial ants parameters, create pheromone trails
For Iter = 1:maxIterations
  For Ant = 1:maxAnts
    Each Ant built Solutions
    Objective Function Evaluation
  End
Update Pheromones on trails
End
```

Fig. 9 Procedure of the ACO

The basic procedural steps of the ACO optimization model are organized as follows:

- Ant colony population initialization
- Stochastic ant movement on the search space
- Examination of candidate solutions at each ant
- Pheromone update based on solution quality and reinforcement mechanisms.

The ACO algorithm has been widely applied to optimization and control problems, ranging from solving the

Traveling Salesman Problem (TSP) for optimal path-finding [22] and job scheduling optimization to network synchronization for improving efficiency in computer and telecommunications networks. Furthermore, ACO has been used for PID controller tuning in control systems [23], energy management in microgrids, and obtaining higher precision in image processing and pattern recognition tasks by using an optimised segmentation algorithm. In this paper, ACO is introduced to solve the problem of microgrids with inertia scarcity by optimizing VSG for both angle and frequency control. The optimal parameters of the generator are of great significance for the stability and dynamic response of the system, which directly affects the energy security and reliability of the microgrid.

3.2. Objective Function for Optimization of Frequency in Microgrid

The lack of inertia in islanded microgrid operations is a key issue that affects the frequency of response to load and generation changes. The VSG control scheme plays a pivotal role in approximating the natural electromechanical properties of a synchronous generator in IBR-GFM and augmenting the system inertia and frequency response. The VSG dynamic behavior is mainly determined by two important parameters: the virtual inertia constant (J) and the damping coefficient (D).

- J: Control the inertia response of the system and measure the ability of the system to resist frequency changes during dynamic events.

- D: Controls frequency oscillation attenuation and the settling time needed to stabilize frequency after disturbances.

The fine-tuning of J and D is very important for the dynamic behavior of VSG, reducing frequency deviation and improving microgrid stability.

Therefore, the optimisation of such parameters is presented in this work as a structural objective function to enhance the robustness and performance of VSG-based MG systems.

$$Min\ f(J,D) = \int_0^T |\Delta f(t)|\ dt - 0.01 \times (J^2 + D^2) \quad (15)$$

In which:

$\Delta f(t) = f(t) - f_{ref}$ represents the frequency deviation from its nominal value.

T denotes the total simulation time.

Subject to the following constraints:

$$Jmax_{min} \quad (16)$$

$$Dmax_{min} \quad (17)$$

Where:

J_{min}, J_{max} establish the minimum and maximum limits for the virtual inertia constant.

D_{min}, D_{max} delineate the boundaries for the frequency damping coefficient.

3.3. Implementation of ACO in VSG Optimization

The control parameter optimization of VSG is a key part of improving the frequency regulation ability of the power system [24, 25]. In order to achieve dynamic performance, VSG's key parameters, i.e., J and D, are estimated by the ACO algorithm. For this purpose, each ant behaves as an autonomous searching agent. It explores the solution space in a systematic manner in order to locate values of l for which frequency deviations are the least and improve system stability.

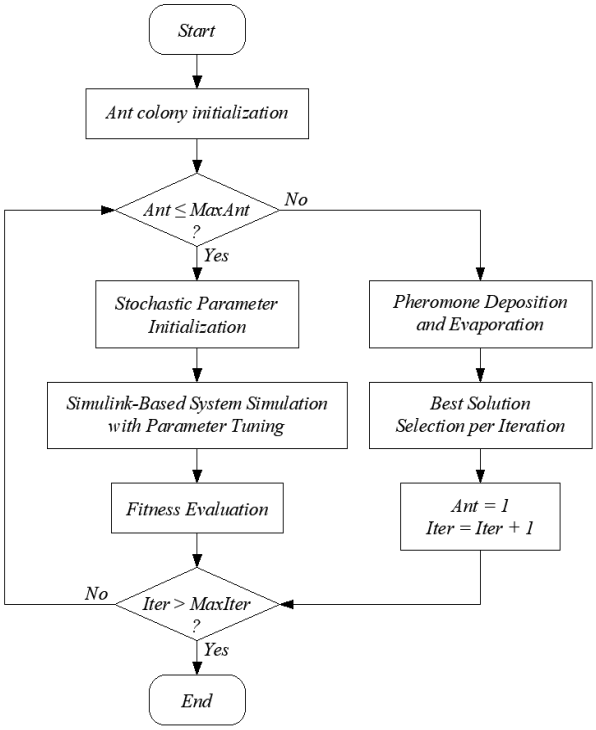

Fig. 10 Flowchart of the ACO algorithm for optimizing parameters J and D

The optimization procedure is programmed in Matlab, and the parameter values are moved back and forth while being tested in dynamic Simulink simulations. The purpose function measures the transient response of the system, leading the search to values of parameters that are instrumental in the reduction of frequency oscillation and settling time. The repeated manner in which the optimization is performed, the pheromone updating, guarantees the progress of the search process becoming towards an optimal solution , and the search process is efficient in the balance between exploration and exploitation.

3.3.1. Phase 1-Initialization of the Ant Colony

The optimization process begins with the initialization of a population consisting of mmm ants. Each ant represents a candidate solution in the form of a randomly selected pair of values for J and D within the defined constraint bounds. Additionally, initial algorithm parameters must be specified to ensure the simulation of natural ant behavior, including:

α : Weight coefficient of pheromone influence
β : Weight coefficient of heuristic information
ρ : Pheromone evaporation rate
Q : Pheromone intensity constant

3.3.2. Phase 2-Probability-Based Movement of Ants

At each stage of the optimization process, ants traverse the solution space based on probabilistic transition rules, which incorporate both heuristic information and pheromone concentration to guide the search toward optimal solutions.

The probability of an ant k transitioning from state i to j at time t is defined as:

$$P_{ij}^{(k)}(t) = \frac{[\tau_{ij}]^{\alpha}.[\eta_{ij}]^{\beta}}{\sum_{s\in N_k}[\tau_{ij}]^{\alpha}.[\eta_{ij}]^{\beta}} \quad (18)$$

In which:

P_{ij}^{k} : The set of nodes that an ant can move to.
τ_{ij} : The pheromone concentration on edge *i*.
η_{ij} : The heuristic information associated with the transition.

α và β: Parameters that regulate the influence of pheromone concentration and heuristic information in the decision-making process.

The candidate solutions (*J, D*) generated by the ants are subsequently transmitted to the Simulink environment for frequency response simulation, enabling performance evaluation and iterative refinement of the optimization process.

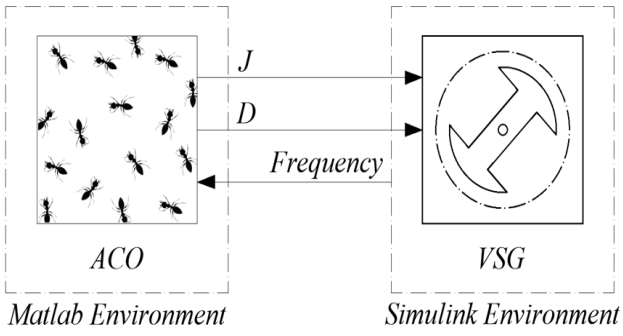

Fig. 3 ACO optimization model

3.3.3. Phase 3-Evaluation of Each Ant's Solution

The simulation process extracts the system's frequency response data and maps it into the MATLAB environment to evaluate the objective function:

$$Min\ f(J,D) = \int_0^T |\Delta f(t)|\ dt - 0.01.(J^2 + D^2) \quad (19)$$

Each ant provides a specific objective function value corresponding to its assigned parameter set. The best-performing ant, determined based on the lowest objective function value, is identified as the temporary optimal solution.

3.3.4. Phase 4-Pheromone Update

Once all ants have generated solutions, they deposit pheromone traces ($\Delta\tau_{ij}$) along their traveled paths. The pheromone update mechanism follows the Equation (20):

$$\tau_{ij} = (1-\rho).\tau_{ij} + \sum_{k=1}^{m}\Delta\tau_{ij}^{(k)} \quad (20)$$

In which:

$\rho$is the pheromone evaporation rate $(0 < \rho \leq 1)$, preventing premature convergence to local optima.

$\Delta\tau_{ij}$ represents the newly deposited pheromone amount, determined as follows:

$$\Delta\tau_{ij}(t) = \sum_{k-1}^{NA}\Delta\tau_{ij}^{(k)} \quad (21)$$

Where:

NA is the total number of ants.

$\Delta\tau_{ij}^{(k)}$ denotes the pheromone deposited by ant k, computed as:

$$\Delta\tau_{ij}^{(k)} = \begin{cases}\frac{Q}{L_k}\\ 0\end{cases} \quad (22)$$

with:

Q being the pheromone intensity constant.

L_k represents the total traveled distance by ant *k*.

This mechanism reinforces pheromone deposition along paths associated with lower frequency deviations, guiding subsequent ants toward more optimal search regions in the solution space.

Following the completion of the parameter optimization process for *J* and *D* using the ACO algorithm, the derived optimal values are integrated into the VSG controller to evaluate its performance within the MATLAB/Simulink simulation environment. The subsequent section presents a

comprehensive analysis of the simulation results, providing empirical validation of the proposed optimization framework's effectiveness in enhancing frequency regulation and system stability.

4. Simulation and Results

Table 1. Ant colony optimization parameters

Number of ants	5
Number of iterations	5
Importance of pheromone	1
Importance of heuristic	2
Pheromone evaporation rate	0.1
Pheromone constant	1
Constraint on J	$0 < J \leq 0.05$
Constraint on J	$0 < D \leq 0.05$

Table 2. IBR system parameters

Filter	
Filter Resistance R_f	1.1 mΩ
Filter Inductance L_f	0.35 mH
Filter Capacitor C_f	0.44 mF
IBR	
Voltage Controller Proportional Gain K_{pv}	6
Voltage Controller Integral Gain K_{iv}	20
Current Controller Proportional Gain K_{pc}	5
Current Controller Integral Gain K_{ic}	50
Active Power Controller Itergal Gain K_{pd}	0.06
Active Power Controller Itergal Gain K_{id}	60

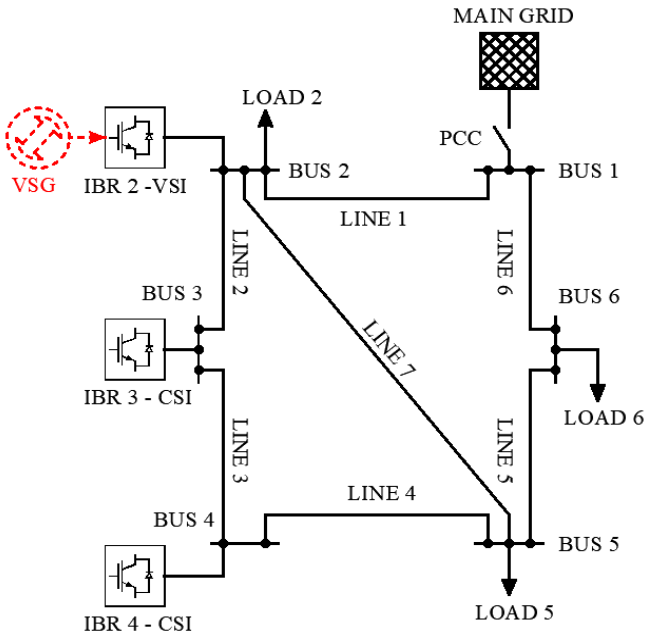

Fig. 12 Autonomous microgrid of 6 bus

Table 3. Line impedance

Line $Zd = Rd + jXd$ (pu), (S_b = 100 kVA; V_b= 0,38 kV)	
Line 1	0.05 + j0.055 pu
Line 2	0.10 + j0.15 pu
Line 3	0.20 + j0.25 pu
Line 4	0.10 + j0.15 pu
Line 5	0.20 + j0.25 pu
Line 6	0.05 + j0.1 pu
Line 7	0.10 + j0.15 pu

Table 4. Load capacity

Load 2	90 + j20 kVA
Load 5	120 + j30 kVA
Load 6	150 + j30 kVA

Results of the objective function using the ACO and PSO algorithms are compared in Figure 13. The experimental results show that ACO has better performance on convergence speed and solution quality than PSO. In fact, ACO has a quicker rate of initial convergence, in which the value of the objective function is dramatically reduced, and it is closer to the optimal region when compared to PSO. Contrarily, PSO improves at a slower rate. The final comparison indicates that the overall value of the objective function obtained using ACO is even lower than using PSO, so a more optimized optimal solution is found. Furthermore, ACO has more stability across generations. Compared to when the algorithm is near the optimum solution, the optimal function value is still fixed with less oscillations, but PSO is generally stuck or more unstable. This demonstrates ACO's improved capacity to escape local optima, as it still refines its solution rather than getting stuck at some suboptimal solution, as seen in PSO. Figures 14 and 15 show the movement traces of single searching agents in the solution space for the PSO and ACO, respectively. A comparison of these numbers shows the different search strategies of PSO and ACO. The movement of particles is a bit more structured and directed, as can be seen from the linearized trajectories converging to unlike search zone in Figure 14. In comparison, Figure 15 has a more scattered search, and they move non-linearly or differently in each direction.

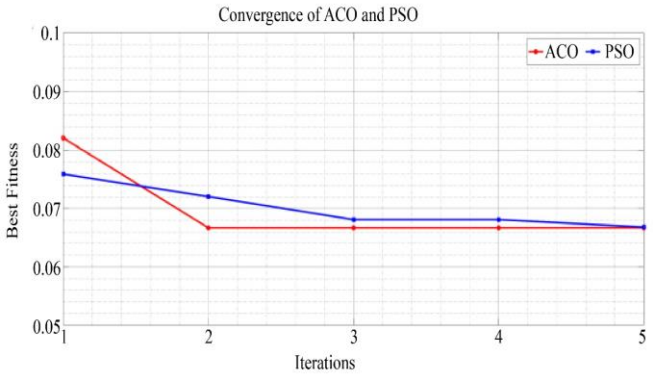

Fig. 13 Comparison of objective function values between ACO and PSO algorithms

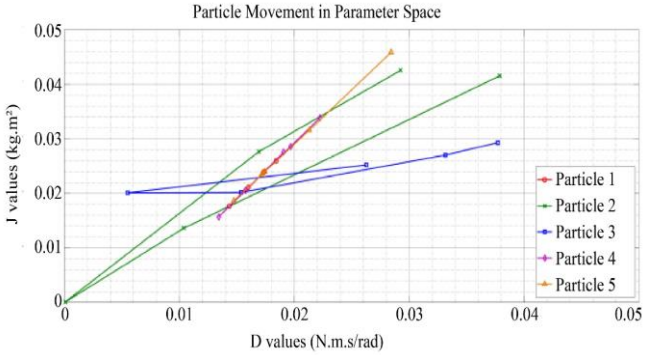

Fig. 14 Movement process of each particle in the search space

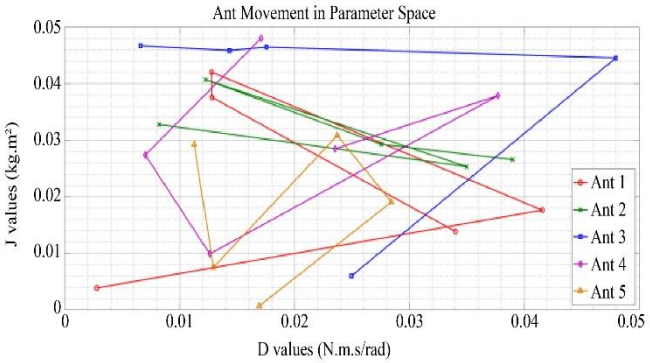

Fig. 15 Movement process of each ant in the search space

This means that ACO has a higher exploration ability, which helps them search space effectively and avoid premature convergence with some local min. On the other hand, PSO direction is more deterministic, and this purposeful movement may make the algorithm overly selective in its search; hence, the danger of reaching local minima is greater. Conversely, ACO maintains a balanced approach between exploration and exploitation, allowing it to efficiently search for optimal solutions in complex, multimodal objective functions. Figure 16 shows the simulated active power dynamic in the system, the power injected by each IBR to satisfy changes in load. Two-step commands for the load power at 3 seconds and 7 seconds are given to model the transient disturbance and to the response of IBR units at the changeable load power.

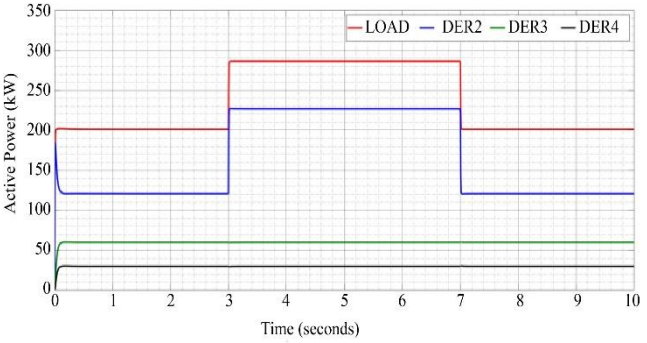

Fig. 16 Active power characteristic curve

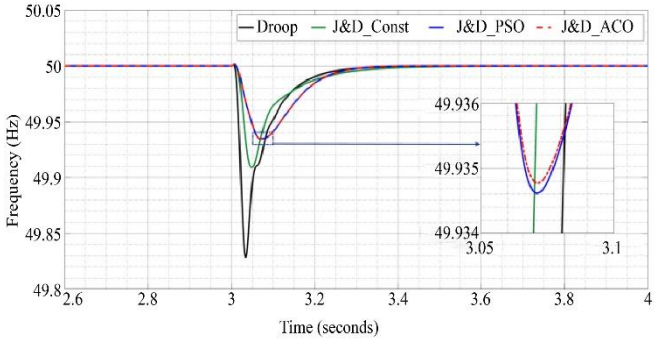

Fig. 17 Frequency characteristic curve at 3s during load power increase

Results show that IBR3 and IBR4 only provide small power sharing between sources as the secondary source to supply load and do not significantly affect the primary power-sharing of the MG. In the meantime, the evident power hump in IBR2 also indicates its crucial position in balancing the power system. This behavior is in congruence with the principle of operation of grid-forming inverters, which ensures voltage and frequency regulation and that power generation does not exceed the allowed limits.

The purpose of this simulation is to assess the efficiency of this VSG in frequency stabilization. It is shown that the ACO is used to optimize VSG control parameters and is capable of obtaining better dynamic responses than conventional methods. This matches the behaviour of grid-forming inverters, which guarantee voltage and frequency control as well as limit the production of power when it goes beyond the imposed limits. The aim of this simulation is to evaluate the performance of this VSG in frequency stabilization. It is also demonstrated that ACO can be helpful in the optimization of VSG control parameters and has the ability to yield much improved dynamic response when compared to traditional approaches.

The simulation frequency response results in Figure 17 further confirm the effectiveness of the proposed control method under a step-up in load power at sub-cycle 3 s. It is found that the proposed method achieves a smaller frequency-deviation amplitude at the time when a power imbalance takes place while a longer settling time is needed.

This result highlights the important function of system inertia in improving transient power frequency performance and stability following disturbances. Notably, the variation of the virtual inertia constant J optimized by ACO and PSO leads to improved frequency oscillation damping compared to the fixed-parameter and conventional droop control approaches.

It also shows that our dynamic control proposed in this study can make the virtual inertia constant J optimized by ACO and PSO so as to achieve better frequency oscillation damping performance, and its frequency oscillation damping is better than the fixed-parameter and the traditional droop.

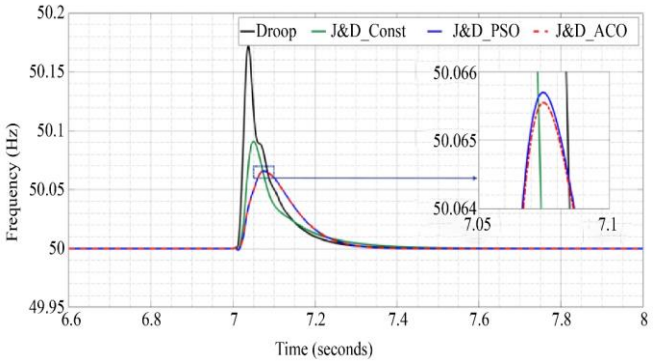

Fig. 18 Frequency characteristic curve at 7s during load power reduction

Nevertheless, for the ACO-optimized parameters, the frequency deviation amplitude is slightly lower than that achieved for PSO, but the difference is small. It is therefore implied that the improvement of ACO in parameter optimization over PSO is not that much better to improve the performance of frequency response. The system frequency response of followers at 7s (showing load reduction event) is shown in Figure 18 to give an indication of the performance of various control techniques. Numerical results show that under conventional droop control there would be significant frequency deviations arising from its intrinsic lack of synthetic inertia support that is essential to system stability. This constraint highlights the notable contribution of virtual inertia in the transient frequency deviation. The VSG fixed-parameter model with specified virtual inertia constant J and virtual damping coefficient D exhibits a fundamental tradeoff between response speed and frequency overshoot. The problem of difficult parameter tuning is caused by the tradeoff between the tedium of adjusting parameters and the need for rapid response and stability, especially when using heuristic optimization. On the other hand, the adaptive controller that-holistically modulate-J and D demonstrates the capability to outperform the fixed-parameter J and D values by adequately attenuating the frequency overshoot, regardless of the increase or decrease of the load of the system. This enhancement shows that appropriate inertia tuning is crucial to the stability of transient frequency offsets. However, increasing the value of J results in better frequency stability to the detriment of longer settling time, which is a tradeoff in its own right for mimicking a synchronous generator. These results highlight the necessity to optimize the virtual inertia gains to tradeoff fast FRR and overshoot mitigation, and thus enhance the overall robustness of the microgrid frequency control.

5. Conclusion

In this paper, the effectiveness of VSG as an emulator for small swings of a synchronous generator is demonstrated by employing it for an emulating conventional synchronous generator. This provides better damping and system stability with changes in load and generation than traditional droop-based control strategies and leads to better voltage and frequency stability in the system. In addition, the VSG control parameters are important to optimize the system performance. To demonstrate the effectiveness of the proposed method, a simulation model in MATLAB/Simulink was created to implement the VSG and ACO-based optimization. It is observed that both fixed-parameter VSG models and conventional droop control show less performance than ACO and PSO-optimized models for frequency deviation attenuation. The comparison between ACO and PSO also shows that the ACO algorithm is better for parameter adjustments because the latter has a pheromone-based search mechanism. Unlike PSO, its search is based on inertia-weighted exploration. ACO uses pheromone trails to direct the search, leading to a more intelligent way of searching, resulting in an efficient exploration of the solution space and reducing the vulnerability to local optima trapping.

Simulation results have proved the dynamic advantage of using the ACO algorithm implemented to search and optimized the control parameters of VSG, which leads to an increment in synthetic inertia in the microgrid and consequently enhances the system stability greatly.

Based on these findings, the emerging trend of interconnecting individual microgrids into a unified Interconnected Microgrid system aimed at improving the reliability and operational flexibility of the entire power network has been gaining increasing attention in recent research. Therefore, an important future direction of this study is to further extend the application of the ACO algorithm to frequency control in Interconnected Microgrid systems, taking into account power flow constraints on the interconnecting lines in order to ensure stable and optimal operation under the complex interconnection conditions of distributed power systems.

Funding Statement

This research was funded by the Hanoi University of Industry under the Scientific Research and Technology Development project, code 12-2023-RD/HĐ-ĐHCN.

Acknowledgments

The authors would like to express their sincere gratitude to Hanoi University of Industry for its support throughout the research process. The authors also appreciate the assistance and valuable discussions provided by colleagues and research collaborators during the preparation of this manuscript.

References

[1] Saad Ahmad et al., "A Review of Microgrid Energy Management and Control Strategies," *IEEE Access*, vol. 11, pp. 21729-21757, 2023. [CrossRef] [Google Scholar] [Publisher Link]

[2] Moslem Uddin et al., "Microgrids: A Review, Outstanding Issues and Future Trends Moslem," *Energy Strategy Reviews*, vol. 49, 2023. [CrossRef] [Google Scholar] [Publisher Link]

[3] Amirnaser Yazdani, and Reza Iravani, *Voltage-Sourced Converters in Power Systems: Modeling, Control, and Applications*, *John Wiley & Sons*, 2010. [Google Scholar] [Publisher Link]

[4] Joan Rocabert et al., "Control of Power Converters in AC Microgrids," *IEEE Transactions on Power Electronics*, vol. 27, no. 11, pp. 4734-4749, 2012. [CrossRef] [Google Scholar] [Publisher Link]

[5] Prabha S. Kundur, and Om P. Malik, *Power System Stability and Control*, 2nd ed., *McGraw-Hill*, 1994. [Google Scholar]

[6] Jia Liu et al., "Enhanced Virtual Synchronous Generator Control for Parallel Inverters in Microgrids," *IEEE Transactions on Smart Grid*, vol. 8, no. 5, pp. 2268-2277, 2017. [CrossRef] [Google Scholar] [Publisher Link]

[7] Chenyang Li et al., "Modelling and Small Signal Stability for Islanded Microgrids with Hybrid Grid-Forming Sources based on Converters and Synchronous Machines," *International Journal of Electrical Power & Energy Systems*, vol. 157, 2024. [CrossRef] [Google Scholar] [Publisher Link]

[8] Lakshmi Satya Nagasri D., and Marimuthu R., "Review on Advanced Control Techniques for Microgrids," *Energy Reports*, vol. 10, pp. 3054-3072, 2023. [CrossRef] [Google Scholar] [Publisher Link]

[9] Sudhir Kumar Singh et al., "Virtual Synchronous Machine Using Ant Colony Optimization in Inverter Interfaced Distributed Generation (IIDG)," *Journal of Electrical Engineering & Technology*, vol. 18, no. 1, pp. 167-179, 2023. [CrossRef] [Google Scholar] [Publisher Link]

[10] Long Phan-Van et al., "A Comparison of Different Metaheuristic Optimization Algorithms on Hydrogen Storage-Based Microgrid Sizing," *Energy Reports*, vol. 9, pp. 542-549, 2023. [CrossRef] [Google Scholar] [Publisher Link]

[11] Yongli Zhu et al., "Optimization of Battery Energy Storage to Improve Power System Oscillation Damping," *IEEE Transactions on Sustainable Energy*, vol. 10, no. 3, pp. 1015-1024, 2018. [CrossRef] [Google Scholar] [Publisher Link]

[12] Thongchart Kerdphol et al., "Virtual Inertia Control-Based Model Predictive Control for Microgrid Frequency Stabilization Considering High Renewable Energy Integration," *Sustainability*, vol. 9, no. 5, pp. 1-21, 2017. [CrossRef] [Google Scholar] [Publisher Link]

[13] Jong Ju Kim, and June Ho Park, "A Novel Structure of a Power System Stabilizer for Microgrids," *Energies*, vol. 14, no. 4, pp. 1-33, 2021. [CrossRef] [Google Scholar] [Publisher Link]

[14] Mohamed Yaich et al., "Metaheuristic Optimization Algorithm of MPPT Controller for PV System Application," *The International Conference on Energy and Green Computing (ICEGC'2021)*, vol. 336, pp. 1-6, 2022. [CrossRef] [Google Scholar] [Publisher Link]

[15] Jingyang Fang et al., "On the Inertia of Future More-Electronics Power Systems," *IEEE Journal of Emerging and Selected Topics in Power Electronics*, vol. 7, no. 4, pp. 2130-2146, 2019. [CrossRef] [Google Scholar] [Publisher Link]

[16] Paul Denholm et al., "Inertia and the Power Grid: A Guide Without the Spin," *National Renewable Energy Laboratory*, Golden, CO, 2020. [Google Scholar]

[17] Mpeli Rampokanyo et al., "Impact of High Penetration of Inverter-based Generation on System Inertia of Networks," *Electra CIGRE*, 2021. [Google Scholar] [Publisher Link]

[18] Amirnaser Yazdani, and Reza Iravani, "A Unified Dynamic Model and Control for the Voltage-Sourced Converter under Unbalanced Grid Conditions," *IEEE Transactions on Power Delivery*, vol. 21, no. 3, pp. 1620-1629, 2006. [CrossRef] [Google Scholar] [Publisher Link]

[19] Marco Dorigo, and Thomas Stützle, *Ant Colony Optimization*, MIT Press, 2004. [Online]. Available: https://mitpress.mit.edu/9780262042192/ant-colony-optimization/

[20] Marco Dorigo, and Gianni Di Caro, "Ant Colony Optimization: A New Meta-Heuristic," *Proceedings of the 1999 Congress on Evolutionary Computation-CEC99*, Washington, DC, USA, vol. 2, 1992. [CrossRef] [Google Scholar] [Publisher Link]

[21] MarcoDorigo, Vittorio Maniezzo, and Alberto Colorni, "Ant System: Optimization by a Colony of Cooperating Agents," *IEEE Transactions on Systems, Man, and Cybernetics, Part B (Cybernetics)*, vol. 26, no. 1, pp. 29-41, 1999. [CrossRef] [Google Scholar] [Publisher Link]

[22] Dorian Gaertner, and Keith Clark, "On Optimal Parameters for Ant Colony Optimization algorithms TSP classifications," *Proceedings of the 2005 International Conference on Artificial Intelligence IC-AI*, Las Vegas, Nevada, USA, pp. 83-89, 2005. [Google Scholar] [Publisher Link]

[23] Ibtissem Chiha, Noureddine Liouane, and Pierre Borne, "Tuning PID Controller Using Multiobjective Ant Colony Optimization," *Applied Computational Intelligence and Soft Computing*, vol. 2012, no. 1, pp. 1-7, 2012. [CrossRef] [Google Scholar] [Publisher Link]

[24] Mohd Hanif Othman et al., "Genetic Algorithm-Optimized Adaptive Network Fuzzy Inference System-Based VSG Controller for Sustainable Operation of Distribution System," *Sustainability*, vol. 14, no. 17, pp. 1-16, 2022. [CrossRef] [Google Scholar] [Publisher Link]

[25] Qian Chen et al., "Analysis of Grid-Connected Stability of VSG-Controlled PV Plant Integrated with Energy Storage System and Optimization of Control Parameters," *Electronic*, vol. 13, no. 7, pp. 1-18, 2024. [CrossRef] [Google Scholar] [Publisher Link]